Experimental investigation of erosion processes downstream of block ramps in mild curved channels

STEFANO PAGLIARA (IAHR Member), Professor, *DESTEC - Department of Energy, Systems, Territory and Construction Engineering, University of Pisa, Pisa, Italy*

Email: s.pagliara@ing.unipi.it

MICHELE PALERMO (IAHR Member), Senior Researcher, *DESTEC - Department of Energy, Systems, Territory and Construction Engineering, University of Pisa, Pisa, Italy*

Email: michele.palermo@ing.unipi.it (author for correspondence)

*Telephone number:*0039 050 2217929

DEEP ROY, PhD Student, *DESTEC - Department of Energy, Systems, Territory and Construction Engineering, University of Pisa, Pisa, Italy*

Email: d.roy1@studenti.unipi.it

Abstract: Eco-friendly low-head river restoration structures such as block ramps are of paramount importance with regard to the control of sediment grade in rivers, particularly in the mountains. They also help in the stabilization of river bed and prevent damages due to excessive downstream erosion by dissipating flow energy. Although the hydraulic characteristics of block ramps in straight channels have been thoroughly studied, there are very less studies dealing with the analysis of scour mechanism downstream of block ramps in curved channels. In fact, to the authors' best knowledge, there are no studies till date investigating the scour process downstream of block ramps in river bends, involving the effect of tailwater and ramp bed slope. Therefore, this study aims to analyze the hydraulic behaviour of block ramps placed at various positions on a curved channel incorporating the effects of the mentioned parameters. Furthermore, the equilibrium morphology of the resulting downstream scour has

been analyzed and classified. A dedicated hydraulic model was constructed, and a large range of in-situ hydraulic conditions were simulated. Tests were carried out varying ramp slope and locating the structure at different positions along the channel bend. Data analysis revealed that the scour morphology is essentially three-dimensional and depends on flow characteristics, tailwater level and slightly on its location. Finally, a useful design relationship was also developed to evaluate the maximum scour depth taking into consideration the effect of channel curvature and the tailwater level.

Key words: Block ramp, flow pattern, river curvature, scour morphology

1. Introduction

Training and maintenance of rivers is a major concern in the present decade, especially in the mountainous region where they are characterized by abrupt slope changes. Moreover, river meandering often takes place in flat areas and it is a complex phenomenon characterized by asymmetric flow distribution and bed erosion. Therefore, careful attention should be given to those structures used to provide sediment control and flow energy dissipation. In this regard, block ramps, rock weirs and stepped gabion weirs are eco-friendly structures which are frequently used for river restoration. However, a scour process generally takes place in the downstream stilling basin, resulting in a serious threat to structure stability. Thus, the hydraulic characteristics and scour mechanism should be studied to efficiently design the downstream stilling basin and avoid structural failure.

The investigation of such scour phenomena was undertaken by several researchers [e.g., 1-9, 11, 19, 22]. In particular, Veronese [22] carried out one of the first studies on the scour characteristics downstream of spillways, resulting in the identification of the main parameters controlling the scour phenomenon. Breusers and Raudkivi [4], Hoffmans and Verheij [9] and Mason and Arumugam [11] compared several empirical relationships to predict the magnitude of maximum scour depth for different type of structures usually adopted in controlling sediment load in rivers, concluding that they are not universally applicable but dependent on available experimental data and on geometric configurations tested.

To overcome such limitations, recent studies have proposed semi-theoretical or fully theoretical approaches, either based on Newton's second law (Hoffmans [8]) or on the phenomenological theory of turbulence (Bombardelli et al. [2]). Nevertheless, it is worth mentioning that, to date, such approaches are still not able to provide universal tools for all the possible structure configurations, hydraulic conditions and in situ scenarios, as they mainly

focus on scour processes caused by plunging jets. Therefore, empirical approaches still represent a valid alternative for complex structures like block ramps.

For this structure typology, the first two authors conducted systematic experimental studies in straight channels, focusing on the effects of protection rock sills, bed material gradation, tailwater level and stilling basin geometry on scour depth (Pagliara and Palermo [14], [15] and [16], Pagliara et al. [18]).

Nevertheless, scour process downstream of block ramps located in curved channel still represents a challenging problem. In fact, only one preliminary study (see Pagliara et al. [20]) analyzed the effect of channel curvature and inflow conditions on scour downstream of mildly sloped block ramps and for protected stilling basin. In that study, authors compared model results with field measurements taken in correspondence with a series of block ramps in the Porebianka river (Poland), and proposed the following empirical equation:

$$Z_m = 0.58 S_0^{0.75} \mathrm{F}_{d90}^{1.8} \quad (1a)$$

$$Z_{msc} = 0.912 Z_m (1 + B/R)^{2.82} \quad (1b)$$

valid for S_0 =0.083, $1.0 \leq \mathrm{F}_{d90} \leq 3.75$, and $0 \leq B/R \leq 0.083$.

Note that $Z_m = z_{max}/h_1$ is the maximum non-dimensional scour depth in straight channels with uniform bed material and it is calculated with Eq. (1a) proposed by Pagliara and Palermo [14], where z_{max} is the maximum scour depth and h_1 the water depth at the ramp toe. Conversely, $Z_{msc} = z_{max}/h_1$ is the maximum non-dimensional scour depth in curved channels. S_0 is the ramp slope and $\mathrm{F}_{d90} = V_1/(g' d_{90})^{1/2}$ is the densimetric Froude number, where $g' = g[(\Delta\rho)/\rho]$ is the reduced gravitational acceleration, $\Delta\rho$ is the reduced sediment density $\rho_s - \rho$, ρ_s and ρ are the bed sediment and water densities, V_1 is average flow velocity at ramp toe, d_{90} is the diameter for which 90% of sediment is finer, B is the channel width and R is the radius of curvature. It is worth mentioning that Eq. (1b) does not depend on S_0 and the downstream tailwater h_0, as Pagliara et al. [20] did not investigate the effect of these two parameters.

Therefore, this study was conducted to partially fulfil this gap of knowledge. In fact, to the best of authors' knowledge, this is the first study that analyzes the effects of both h_0 and S_0 on the scour mechanism downstream of a block ramp in curved channels. To do so, experimental tests were carried on by varying ramp slope and by placing the structure at different positions in the channel bend. This last aspect is also relevant and novel for steep sloped ramps. Based on the analysis of experimental data, we were able to derive a useful empirical relation that represents a valid and unprecedented tool to predict the maximum scour depth for such large range of hydraulic conditions and geometric configurations. Furthermore, we provide a classification of the equilibrium scour morphology, depending on the approaching flow conditions and channel geometry. The knowledge of equilibrium morphology shape and its geometric characteristics could be valuable for practical applications. In fact, it can furnish some useful information to protect river banks.

Figure 1 shows the main geometric and hydraulic parameters, where l_0 indicates the maximum length of scour hole and z_M denotes the ridge height.

2. Experimental methodology

57 experimental tests (see Table 1) were conducted in a 0.5 m wide, 0.5 m deep, and 10 m long channel. The channel was characterized by a straight branch followed by a curved one (with radius of curvature R = 6 m, see Fig. 2). Reference tests were conducted in the straight part of the channel. Subsequently, other tests (termed second series in the following) were carried on by locating the block ramps at different positions along the channel bend, i.e., at the beginning, at one-third and at two-third of the channel bend (α = 0, 0.256, 0.512 rad, where α is the angle subtended by the arc extending from the beginning of the curved part of the channel

to the block ramp location, see Fig. 2). (Note that the angle of the arc extending from the beginning to the end of the bend is $3\alpha = 0.768$ rad.)

Block ramps were modeled by using inox sheets on which a granular material was glued ($d_{50} = 22.7$ mm and non-uniformity parameter $\sigma=(d_{84}/d_{16})^{0.5}=1.19$). One uniform cohesionless material was used for channel bed ($d_{50} = 1.75$ mm, $d_{90} = 2.20$ mm, $\sigma = 1.17$, and $\rho_s = 2214$ kg/m^3).

In reference tests, three different ramp slopes S_0 were simulated (i.e., $S_0 = 0.083$, 0.167 and 0.25) and the discharge Q varied between 0.006 m^3/s and 0.0176 m^3/s. While, in the second series of tests, S_0 ranged between 0.083 and 0.25 (including some selected additional tests conducted for $S_0 = 0.2$) and the discharge Q between 0.006 m^3/s and 0.0155 m^3/s.

Before starting experimental tests, the channel bed was ensured to be horizontal. Both the discharge and the downstream tailwater depth were kept constant during the test and the tailwater depth was regulated using a sluice gate located at the downstream end of the channel.

Some preliminary tests lasting up to 6 hours were conducted to establish the time duration to reach the equilibrium configuration. They allowed us to verify that the scour morphology after 6 hours was essentially the same of that obtained after 2 hours, under the same hydraulic conditions and geometric configurations, i.e., $[z_{max(t=6\ h)} - z_{max(t=2\ h)}]/z_{max(t=6\ h)} \leq 0.05$, where $z_{max(t=6\ h)}$ and $z_{max(t=2\ h)}$ are the maximum scour depths after 6 and 2 hours from the tests beginning, respectively. Therefore, the equilibrium configuration was assumed to be reached after approximately 120 minutes from the beginning of the test.

For all the tests, the hydraulic jump was completely confined in the stilling basin, thus resulting in a F_{MB} hydraulic jump type (free jump in mobile bed), according to the classification proposed by Pagliara and Palermo [16].

Measurements of both water surface level and bed morphology were taken by using a point gauge of 0.1 mm accuracy. In particular, the methodology proposed by Hughes and Flack

[10] was adopted to measure h_1 (see also Pagliara and Palermo [17] and Palermo and Pagliara [21] for details).

All the tests were carried out under the clear water condition. Figure 3, we show two pictures of the experimental apparatus, highlighting the flow asymmetry at the ramp toe due to the channel curvature.

3. Results and discussion

3.1 *Scour depth*

Bombardelli et al. [2] and Hoffmans [8] found that the jet diffusion length ($z_{max}+h_0$) is a key factor in scour phenomena caused by plunging jets, corroborating the findings of Bormann and Julien [3] for grade-control structures. Following such approaches and considering the specific geometric configuration of tested structures, the variable $z_{max}+h_0$ can be assumed dependent on the following parameters:

$$z_{max} + h_0 = f(Q, h_1, B, g, \Delta\rho, \rho, d_{90}, \alpha, R, S_0) \quad (2)$$

To derive an empirical relationship for scour depth estimation, we performed a detailed dimensional analysis (see Appendix for details). Namely, by assuming Q, h_1 and ρ as repeating variables, we obtained the following non-dimensional functional relationship:

$$\frac{z_{max}+h_0}{h_1} = f\left(\frac{B}{h_1}, \frac{h_1^5 g}{Q^2}, \frac{\Delta\rho}{\rho}, \frac{d_{90}}{h_1}, \alpha, \frac{R}{h_1}, S_0\right) \quad (3)$$

By re-arranging some of the non-dimensional groups of Eq. (3), it is easy to obtain the following Eq. (4):

$$\frac{z_{max}+h_0}{h_1} = f\left(\frac{B}{h_1}, F_{d90}, \frac{\Delta\rho}{\rho}, \frac{d_{90}}{B}, \alpha, \frac{B}{R}, S_0\right) \quad (4)$$

It is worth mentioning that tests were conducted in the following ranges of non-dimensional groups: $9.1 \le B/h_1 \le 36.7$, $1 \le F_{d90} \le 6$, $\Delta\rho/\rho$=1.214, d_{90}/B=0.0044, $0 \le \alpha \le 0.512$,

$0 \leq B/R \leq 0.083$, and $0.083 \leq S_0 \leq 0.25$. $\Delta\rho/\rho$ and d_{90}/B being constant, and considering that the effect of the non-dimensional group B/h_1 was found negligible, Eq. (4) can be further re-arranged as follows:

$$\frac{z_{max}+h_0}{h_1} = f\left(F_{d90}, \alpha, \frac{B}{R}, S_0\right) \quad (5)$$

The maximum scour depth decreases with h_0, for identical inflow conditions and ramp geometry. This occurrence is mainly due to the fact that the diffusion length of the jet exiting the ramp toe increases with h_0, thus reducing the shear stress acting on the granular channel bed material (see also Bombardelli et al. [2], Bormann and Julien [3], Hoffmans [8]). Furthermore, we tested two different non-dimensional B/R values, i.e., B/R=0 (R=∞, straight channel) and B/R=0.083 (R=6 m). Therefore, it is appropriate to keep the non-dimensional parameter B/R in the governing functional relationship.

For straight channels, Eq. (5) can be further simplified, as the parameters α and R/B does not appear in it. Pagliara and Palermo [16] conducted an extensive analysis of the scour process occurring downstream of block ramps in straight channels and proposed the following Eq. (6):

$$(z_{max} + h_0)/h_1 = (11.64S_0 + 0.7)\, exp[(-0.64S_0 + 0.17)F_{d90}] \quad (6)$$

valid for $1 \leq F_{d90} \leq 4$ and $0.083 \leq S_0 \leq 0.25$. Pagliara et al. [16] also found that Eq. (6) does not depend on the bed sediment gradation for $\sigma < 2.8$.

In the present study, reference tests were conducted for F_{d90} values up to 6, but in the same range of ramp slope tested by Pagliara and Palermo [16]. Thus, the first step of data elaboration consisted in the extension of the range of applicability of Eq. (6) to F_{d90} values up to 6. Figure (4) shows that Eq. (6) can be successfully applied for higher F_{d90} values ($R^2 = 0.85$). Therefore, it can be assumed to be valid for $1 \leq F_{d90} \leq 6$ and $0.083 \leq S_0 \leq 0.25$.

The second step of data elaboration consisted in the analysis of the scour process downstream of block ramps located in the curved part of the channel (second series of experimental tests). Namely, the effect of the parameters α and B/R on the variable $(z_{max}+h_0)/h_1$ was analyzed. To do so, data points were plotted in a parametric graph $(z_{max}+h_0)/h_1$ vs F_{d90} (see Fig. 5) and were distinguished according to the ramp slope S_0 and ramp longitudinal position (α) in the curve. Experimental evidence revealed that: 1) $(z_{max}+h_0)/h_1$ increases with B/R for otherwise identical conditions, i.e., z_{max} decreases with R for the same inflow conditions and same tailwater depth h_0 (this occurrence is also in agreement with the findings of Pagliara and Kurdistani [12] and Pagliara et al. [13], who tested other low-head structures typologies in curved channels); 2) the effect of α appears to be negligible, i.e., z_{max} is slightly influenced by α, implying that Eq. (5) can be further simplified as follows:

$$(z_{max} + h_0)/h_1 = f\,(F_{dxx}, S_0, B/R\,) \qquad (7)$$

Nevertheless, it is worth mentioning that, when a block ramp is located in a river bend, the scour morphology becomes three-dimensional. Thus, the shear stress distribution on the channel bed is asymmetric, resulting in an increase of the erosive action in correspondence with the outer bend. In fact, scour process mainly takes place on one side of the channel and a preferential flow path can establish, depending on both downstream water level and flow discharge.

The position of the block ramp along the channel bend can also influence the inflow conditions. When a block ramp is located at the beginning of a river bend and preceded by a straight branch, the upstream kinematic flow field is essentially symmetric and it becomes asymmetric downstream of the structure, because of the flow acceleration.

Conversely, if a block ramp is located within the river bend, both the upstream and downstream kinematic flow fields are asymmetric. For mild ramp slopes, the effect of the upstream kinematic flow field was found negligible in terms of maximum scour depth by

Pagliara et al. [20]. Namely, z_{max} does not significantly vary with respect to that occurring when the block ramp is located at the beginning of the channel bend, under identical hydraulic inflow conditions. This experimental evidence confirms that $(z_{max}+h_0)/h_1$ does not depend on α and corroborates Eq. (7).

Nevertheless, the downstream kinematic flow field asymmetry is more prominent if R reduces (i.e., for more curved channels), reflecting an increase of the local shear stress and resulting in a deeper scour hole. Furthermore, higher discharges, river curvature and ramp slopes contribute to exacerbate such behaviour. Scour mainly occurs in correspondence with the outer channel wall, and thereby can remain laterally confined by a longitudinally extended ridge. Flow characteristics appear similar to that established within a symmetrically/asymmetrically enlarged stilling basin (see Pagliara et al. [18]). The flow entering the stilling basin is not uniformly distributed, but concentrated close to the outer channel wall. Following the approach adopted by Pagliara et al. [18] for expanded stilling basins, an equivalent densimetric Froude number $\dot{F}_{d90}$ has been introduced, allowing us to take into account the local shear stress increase and to preserve the algebraic form of Eq. (6). $\dot{F}_{d90}$ is defined as the densimetric Froude number causing the same z_{max} in a straight channel under identical hydraulic conditions and ramp configuration (i.e., for same h_0, h_1, Q and S_0). The analysis of experimental data allowed us to derive the following expression for $\dot{F}_{d90}$:

$$\dot{F}_{d90} = F_{d90}(1 + B/R)^{(1548{S_0}^2 - 360.2S_0 + 24)} \quad (8)$$

valid for $1 \leq F_{d90} \leq 6$, $0.083 \leq S_0 \leq 0.25$ and $0 \leq B/R \leq 0.083$ (R^2=0.93). It is worth mentioning that $\dot{F}_{d90} = F_{d90}$ for B/R=0 (i.e., straight channel) and it increases with S_0. Therefore, Eq. (6) can be re-written as follows:

$$(z_{max} + h_0)/h_1 = (11.64S_0 + 0.7)\exp\left[(-0.64S_0 + 0.17)\dot{F}_{d90}\right] \quad (9)$$

and it is valid for $1 \leq F_{d90} \leq 6$, $0.083 \leq S_0 \leq 0.25$ and $0 \leq B/R \leq 0.083$.

Our analysis assessed the prediction capability of Eq. (9) at equilibrium conditions. In particular, we validated our equation with all experimental data (see Figure 6). Regardless of the channel curvature and block ramp position, Eq. (9) predicts experimental data reasonably well. It is worth mentioning that the variable $\dot{F}_{d90}$ causes a shift of the second series data point abscissa towards higher values, reflecting the shear stress increase in correspondence with the channel bend. Finally, measured data of the variable $(z_{max}+h_0)/h_1$ were compared against those calculated by using Eq. (9). The result of the comparison is shown in Figure 7.

3.2 *Scour morphology*

A detailed analysis of equilibrium morphologies revealed that they depend on approaching flow conditions, tailwater depth and channel geometry. In fact, the power of the jet exiting the ramp toe increases with discharge, resulting in an increase of shear stresses acting on the movable bed. Conversely, shear stress scales with $1/(z_{max}+h_0)$ (see Bombardelli et al. [2]), thus scour depth reduces with h_0. Finally, channel curvature also plays a fundamental role, by causing a flow acceleration and an asymmetric distribution of flow discharge in the stilling basin. It is worth mentioning that channel curvature and downstream water level also affect hydraulic jump, whose features become essentially 3D, especially for high h_0 and Q values (see Fig. 3b).

In this study, four types of scour morphologies were distinguished. Type S_a is the reference two-dimensional scour morphology in a straight channel (see Fig. 8a), and types C_a, C_b, and C_c are the three-dimensional scour morphologies occurring in the channel bend (see Figs 8b, c and d, respectively).

Type S_a is characterized by a two-dimensional scour hole, followed by a ridge, whose width is the same as the channel. The maximum scour depth generally occurs in the centre of the channel and it does not vary significantly in the transverse direction. In type C_a, both scour

hole and ridge become asymmetric and longitudinally extended in the outer part of the channel. They are characterized by a certain three-dimensionality, but both the maximum scour depth and ridge height still occur in the central part of the channel (Fig. 8b). In type C_b, the scour hole is significantly three-dimensional and longitudinally extends along the outer channel bend. The maximum scour depth generally occurs close to the outer channel wall and the ridge does not confine the entire scoured area, resulting in sediment deposition in correspondence with the inner part of the channel (Fig. 8c). Furthermore, secondary smaller ridge formations can eventually occur immediately before and after the scour hole, depending on the inflow hydraulic conditions and tailwater depth. Finally, type C_c is similar to the type C_b, but the downstream ridge is much more prominent and confines the entire scour hole (Fig. 8d). Namely, the ridge starts forming from the inner wall of the channel and then extends up to the outer. Figure 9 shows two contour maps relative to scour types C_b and C_c. They illustrate the equilibrium morphologies obtained in two different tests characterized by similar hydraulic conditions.

The analysis of experimental data allowed us to establish the existence fields of scour types C_a, C_b and C_c, depending on the parameters R/h_0, $\dot{F}_{d90}$ and α (see Fig. 10). For all tested α values, type C_a occurs for lower tailwater depths and low flow discharges. In fact, in such conditions, the hydraulic jump is quasi-2D and a prominent ridge forms downstream, limiting the scour hole longitudinal extension. By increasing the tailwater depth and the flow discharge, hydraulic jump becomes essentially 3D and scour type C_b takes place. In particular, the asymmetry of the velocity distribution results in a preferential flow path formation in correspondence with the outer channel bank, causing a lateral extension of the scoured area. A further increase of h_0 causes the transition from type C_b to type C_c, as it facilitates sediment deposition and ridge formation that confines the entire scoured area.

The location of the ramp within the channel bend also plays a relevant role. Namely, when $\alpha = 0$ rad, a lower tailwater is required for the transition from type C_a to types C_b and C_c, for otherwise identical conditions. Conversely, scour type C_c does not occur for $\alpha = 0.512$ rad. In fact, for higher α values, the velocity field asymmetry is fully developed both upstream and downstream of the structures, whereas it only occurs downstream of the structure for $\alpha = 0$ rad.

From a practical point of view, the proposed classification can be helpful in establishing the conditions in which bank protections are required. In fact, we found that maximum scour depth generally occurs close to the outer channel wall for scour types C_b and C_c. Thus, it is reasonable to assume that the risk of bank failure increases when such scour types take place.

Finally, it is worth noting that the classified scour types show significant similitudes with those occurring downstream of other low-head structures, e.g., rock sills and J-hook vanes (see Pagliara and Kurdistani [12] and Pagliara et al. [13]).

4. Conclusion

In this study we analyzed the scour phenomenon downstream of block ramps, located at different positions in a mildly curved channel. Novel experimental tests were carried out in a dedicated laboratory flume under clear water conditions for uniform bed materials. The first series of tests (reference tests) was conducted by locating the ramp in the straight part of the channel and by varying the ramp slope from 0.083 to 0.25. Whereas, in the second series of tests, scour process occurring downstream of a block ramp located in the curved part of the channel was analyzed.

We found that equilibrium scour morphology is affected by the curvature of channel, tailwater depth and approaching flow conditions. In particular, maximum scour depth increases with channel curvature and decreases with tailwater depth, but it slightly varies with block ramp location in the channel bend. Based on a detailed dimensional analysis, a useful empirical

relationship was derived to estimate the scour depth. It satisfactorily predicts the totality of data.

Four different scour types can be distinguished and classified, depending on channel curvature, tailwater depth, flow discharge and block ramp location. Graphs illustrating the existence fields of different scour types are also provided as function of the non-dimensional river curvature and the equivalent densimetric Froude number. We found that equilibrium morphologies show substantial similitudes with those characterizing other low-head structures.

To the best of authors' knowledge, this is the first systematic study on scour process downstream of block ramps in a curved channel, taking into account both ramp slope and tailwater depth effects on scour features.

Appendix: dimensional analysis

According to Hoffmans (1998) and Bombardelli et al. (2018), the theoretical diffusion length ($z_{max}+h_0$), i.e., the sum of the maximum scour depth, z_{max}, and the water depth over the original sediment bed level, h_0, depends on the following variables:

$$z_{max} + h_0 = f(Q, h_1, B, g, \Delta\rho, \rho, d_{90}, \alpha, R, S_0) \quad \text{(A1)}$$

By assuming Q, h_1 and ρ as repeating variables, we obtain the following non-dimensional groups:

$$\Pi_1 = \frac{z_{max}+h_0}{h_1} \quad \text{(A2)}$$

$$\Pi_2 = \frac{B}{h_1} \quad \text{(A3)}$$

$$\Pi_3 = \frac{h_1^5 g}{Q^2} \quad \text{(A4)}$$

$$\Pi_4 = \frac{\Delta\rho}{\rho} \quad \text{(A5)}$$

$$\Pi_5 = \frac{d_{90}}{h_1} \quad \text{(A6)}$$

$$\Pi_6 = \alpha \tag{A7}$$

$$\Pi_7 = \frac{R}{h_1} \tag{A8}$$

$$\Pi_8 = S_0 \tag{A9}$$

Let's now re-arrange some of the non-dimensional groups Π_i as follows:

$$\Psi_3 = \sqrt{\frac{1}{\Pi_3}\frac{1}{\Pi_2^2}\frac{1}{\Pi_5}\frac{1}{\Pi_4}} = \sqrt{\frac{Q^2}{h_1^2 B^2 g d_{90}\frac{\Delta\rho}{\rho}}} = \frac{V}{\sqrt{g d_{90}\frac{\Delta\rho}{\rho}}} = F_{d90} \tag{A10}$$

$$\Psi_5 = \frac{\Pi_5}{\Pi_2} = \frac{d_{90}}{B} \tag{A11}$$

$$\Psi_7 = \frac{\Pi_2}{\Pi_7} = \frac{B}{R} \tag{A12}$$

Therefore, the non-dimensional functional relationship can be expressed as follows:

$$\Pi_1 = f(\Pi_2, \Psi_3, \Pi_4, \Psi_5, \Pi_6, \Psi_7, \Pi_8) \tag{A13}$$

Considering that B, d_{90}, $\Delta\rho$ and ρ are constant, and that the effect of the non-dimensional group Π_2 (= B/h_1) is negligible, Eq. (A13) can be re-written as:

$$\Pi_1 = f(\Psi_3, \Pi_6, \Psi_7, \Pi_8) \tag{A14}$$

Or, equivalently:

$$\frac{z_{max}+h_0}{h_1} = f\left(F_{d90}, \alpha, \frac{B}{R}, S_0\right) \tag{A15}$$

As α has negligible effect on the variable (z_{max}+h_0)/h_1, the governing functional relationship becomes:

$$\frac{z_{max}+h_0}{h_1} = f\left(F_{d90}, \frac{B}{R}, S_0\right) \tag{A16}$$

Acknowledgments

All authors equally set up the research, analyzed the results, and contributed to writing the paper. This research was funded by University of Pisa Research Project PRA_2018_35

"Approcci eco-sostenibili per i sistemi idrici e la riqualificazione del territorio in ambito urbano".

References

1. Adduce C, Rocca M (2006) Local scouring due to turbulent water jets downstream of a trapezoidal drop: Laboratory experiments and stability analysis. Water Resour Res 42 W02405. https://doi.org/10.1029/2005WR004139

2. Bombardelli FA, Palermo M, Pagliara S (2018) Temporal evolution of jet induced scour depth in cohesionless granular beds and the phenomenological theory of turbulence. Physics of Fluids 30:1-19. https://doi.org/10.1063/1.5041800

3. Bormann E, Julien PY (1991) Scour downstream of grade control structures. J Hydraul Eng 117(5):579-594. https://doi.org/10.1061/(ASCE)0733-9429(1991)117:5(579)

4. Breusers HNC, Raudkivi AJ (1991) Scouring. IAHR Hydraulic structures design manual Balkema, Rotterdam.

5. D'Agostino V, Ferro V (2004) Scour on alluvial bed downstream of grade-control structures. J Hydraul Eng 130(1):1-14. https://doi.org/10.1061/(ASCE)0733-9429(2004)130:1(24)

6. Dey S, Raikar RV (2005) Scour in long contractions. J Hydraul Eng 131(12):1036-1049. https://doi.org/10.1061/(ASCE)0733-9429(2005)131:12(1036)

7. Dey S, Sarkar A (2006) Scour downstream of an apron due to submerged horizontal jets. J Hydraul Eng 132(3):246–257. https://doi.org/10.1061/(ASCE)0733-9429(2006)132:3(246)

8. Hoffmans GJCM (1998) Jet scour in equilibrium phase. J Hydraul Eng 124(4):430–437. https://doi.org/10.1061/(ASCE)0733-9429(1998)124:4(430)

9. Hoffmans GJCM, Verheij HJ (1997) Scour manual. Balkema, Rotterdam

10. Hughes WC, Flack JE (1984) Hydraulic jump properties over a rough bed. J Hydraul Eng 110(12):1755–1772. https://doi.org/10.1061/(ASCE)0733-9429(1984)110:12(1755)

11. Mason PJ, Arumugam K (1985) Free jet scour below dams and flip buckets. J Hydraul Eng 111(2):220-235. https://doi.org/10.1061/(ASCE)0733-9429(1985)111:2(220)

12. Pagliara S, Mahmoudi Kurdistani S (2015) Clear water scour at J-Hook Vanes in channel bends for stream restorations. Ecol. Eng. 83:386–393. https://doi.org/10.1016/j.ecoleng.2015.07.003

13. Pagliara S, Mahmoudi Kurdistani S, Palermo M, Simoni D (2016) Scour due to rock sills in straight and curved horizontal channels. J Hydro-Environ Res 10:12–20. https://doi.org/10.1016/j.jher.2015.07.002

14. Pagliara S, Palermo M (2008a) Scour control downstream of block ramps. J Hydraul Eng 134(9):1376-1382. https://doi.org/10.1061/(ASCE)0733-9429(2008)134:9(1376)

15. Pagliara S, Palermo M (2008b) Scour control and surface sediment distribution downstream of block ramps. J Hydraul Res 46(3):334-343. https://doi.org/10.3826/jhr.2008.3208

16. Pagliara S, Palermo M (2010) Influence of tailwater depth and pile position on scour downstream of block ramps. J Irrig Drain Eng 136(2):120-130. https://doi.org/10.1061/(ASCE)IR.1943-4774.0000132

17. Pagliara S, Palermo M (2015) Hydraulic jumps on rough and smooth beds: Aggregate approach for horizontal and adverse-sloped beds. J Hydraul Res 53(2):243-252. https://doi.org/10.1080/00221686.2015.1017778

18. Pagliara S, Palermo M, Carnacina I (2009) Scour and hydraulic jump downstream of block ramps in expanding stilling basins. J Hydraul Res 47(4):503-511. https://doi.org/10.1080/00221686.2009.9522026

19. Pagliara S, Palermo M, Das R (2016) Eco-friendly countermeasures for enlarged basins erosion. River Res Appl 32(3):441–451. https://doi.org/10.1002/rra.2869

20. Pagliara S, Radecki-Pawlik A, Palermo M, Plesiński K (2017) Block ramps in curved rivers: morphology analysis and prototype data supported design criteria for mild bed slopes. River Res Appl 33(3):427–437. https://doi.org/10.1002/rra.3083

21. Palermo M, Pagliara S (2017) D-jump in rough sloping channels at low Froude numbers. J Hydro-Environ Res 14:150–156. https://doi.org/10.1016/j.jher.2016.10.002

22. Veronese A (1937) Erosioni di fondo a valle di uno scarico. Annali Lavori Pubblici 75(9):717-726 [in Italian]

List of figures

Notation

B = channel width

d_{xx} = size of bed material for which xx% is finer

f = function of

F_d = densimetric Froude number

$\dot{F}_{d90}$ = equivalent densimetric Froude number for curved channels

g = gravitational acceleration

g' = reduced gravitational acceleration

h_1 = approach flow depth at ramp toe

h_0 = downstream tailwater depth

l_0 = scour length

Q = discharge

S_0 = block ramp slope

V_1 = average approach flow velocity at the ramp toe

x = longitudinal coordinate

z = vertical coordinate

z_{max} = maximum scour depth

$z_{max(t=2\ h)}$ = maximum scour depth after 2 hours from the tests beginning

$z_{max(t=6\ h)}$ = maximum scour depth after 6 hours from the tests beginning

z_M = maximum ridge height

Z_m = non-dimensional scour depth in straight channels

Z_{msc} = non-dimensional scour depth in curved channels

R = radius of curvature of the channel

α = location of the block ramp in the curved channel

Π_i = i-th non-dimensional group

ρ = water density

ρ_s = sediment density

σ = sediment non-uniformity parameter

Ψ_i = i-th re-arranged non-dimensional group

Table 1 Experimental test summary

Test	Q [m^3/s]	d_{90} [m]	h_0 [m]	h_1 [m]	R [m]	B [m]	α [rad]	S_0 [-]	z_{max} [m]
1	0.0167	0.0022	0.093	0.038	∞	0.5	0	0.250	0.060
2	0.0098	0.0022	0.057	0.027	∞	0.5	0	0.250	0.051
3	0.0135	0.0022	0.061	0.031	∞	0.5	0	0.250	0.069
4	0.0060	0.0022	0.035	0.022	∞	0.5	0	0.250	0.041
5	0.0135	0.0022	0.069	0.032	∞	0.5	0	0.250	0.055
6	0.0176	0.0022	0.090	0.042	∞	0.5	0	0.250	0.058
7	0.0077	0.0022	0.041	0.025	∞	0.5	0	0.250	0.045
8	0.0107	0.0022	0.053	0.029	∞	0.5	0	0.250	0.053
9	0.0131	0.0022	0.060	0.036	∞	0.5	0	0.167	0.064
10	0.0101	0.0022	0.050	0.026	∞	0.5	0	0.167	0.043
11	0.0060	0.0022	0.057	0.021	∞	0.5	0	0.167	0.024
12	0.0081	0.0022	0.042	0.023	∞	0.5	0	0.167	0.037
13	0.0135	0.0022	0.061	0.036	∞	0.5	0	0.083	0.033
14	0.0098	0.0022	0.049	0.031	∞	0.5	0	0.083	0.034
15	0.0060	0.0022	0.038	0.026	∞	0.5	0	0.083	0.025
16	0.0158	0.0022	0.068	0.040	∞	0.5	0	0.083	0.040
17	0.0080	0.0022	0.043	0.029	∞	0.5	0	0.083	0.024
18	0.0158	0.0022	0.075	0.047	∞	0.5	0	0.083	0.040
19	0.0102	0.0022	0.057	0.039	∞	0.5	0	0.083	0.035
20	0.0102	0.0022	0.049	0.031	6	0.5	0	0.167	0.086
21	0.0060	0.0022	0.036	0.023	6	0.5	0	0.167	0.041
22	0.0080	0.0022	0.055	0.026	6	0.5	0	0.167	0.053
23	0.0102	0.0022	0.053	0.032	6	0.5	0	0.167	0.071
24	0.0126	0.0022	0.061	0.032	6	0.5	0	0.167	0.093
25	0.0155	0.0022	0.088	0.055	6	0.5	0	0.167	0.127
26	0.0155	0.0022	0.079	0.036	6	0.5	0	0.167	0.114
27	0.0126	0.0022	0.044	0.033	6	0.5	0	0.167	0.106
28	0.0060	0.0022	0.018	0.017	6	0.5	0	0.200	0.096
29	0.0080	0.0022	0.020	0.020	6	0.5	0	0.200	0.118
30	0.0120	0.0022	0.036	0.026	6	0.5	0	0.200	0.140
31	0.0120	0.0022	0.072	0.034	6	0.5	0	0.200	0.096
32	0.0100	0.0022	0.054	0.027	6	0.5	0	0.200	0.085
33	0.0080	0.0022	0.039	0.021	6	0.5	0	0.200	0.075
34	0.0150	0.0022	0.058	0.028	6	0.5	0	0.200	0.115
35	0.0060	0.0022	0.057	0.014	6	0.5	0.256	0.250	0.059
36	0.0100	0.0022	0.061	0.017	6	0.5	0.256	0.250	0.106
37	0.0100	0.0022	0.035	0.024	6	0.5	0.256	0.250	0.104
38	0.0150	0.0022	0.069	0.024	6	0.5	0.256	0.250	0.183
39	0.0150	0.0022	0.090	0.025	6	0.5	0.256	0.250	0.153

40	0.0060	0.0022	0.015	0.018	6	0.5	0.256	0.167	0.050
41	0.0060	0.0022	0.018	0.018	6	0.5	0.256	0.167	0.041
42	0.0100	0.0022	0.024	0.024	6	0.5	0.256	0.167	0.087
43	0.0100	0.0022	0.047	0.025	6	0.5	0.256	0.167	0.049
44	0.0150	0.0022	0.035	0.029	6	0.5	0.256	0.167	0.102
45	0.0150	0.0022	0.078	0.034	6	0.5	0.256	0.167	0.070
46	0.0060	0.0022	0.027	0.022	6	0.5	0.256	0.083	0.040
47	0.0100	0.0022	0.037	0.030	6	0.5	0.256	0.083	0.060
48	0.0150	0.0022	0.059	0.034	6	0.5	0.256	0.083	0.087
49	0.0060	0.0022	0.015	0.024	6	0.5	0.512	0.083	0.057
50	0.0100	0.0022	0.037	0.030	6	0.5	0.512	0.083	0.067
51	0.0150	0.0022	0.063	0.040	6	0.5	0.512	0.083	0.088
52	0.0060	0.0022	0.012	0.020	6	0.5	0.512	0.167	0.082
53	0.0100	0.0022	0.048	0.026	6	0.5	0.512	0.167	0.071
54	0.0150	0.0022	0.069	0.032	6	0.5	0.512	0.167	0.116
55	0.0060	0.0022	0.030	0.019	6	0.5	0.512	0.250	0.057
56	0.0100	0.0022	0.048	0.026	6	0.5	0.512	0.250	0.110
57	0.0150	0.0022	0.073	0.032	6	0.5	0.512	0.250	0.152

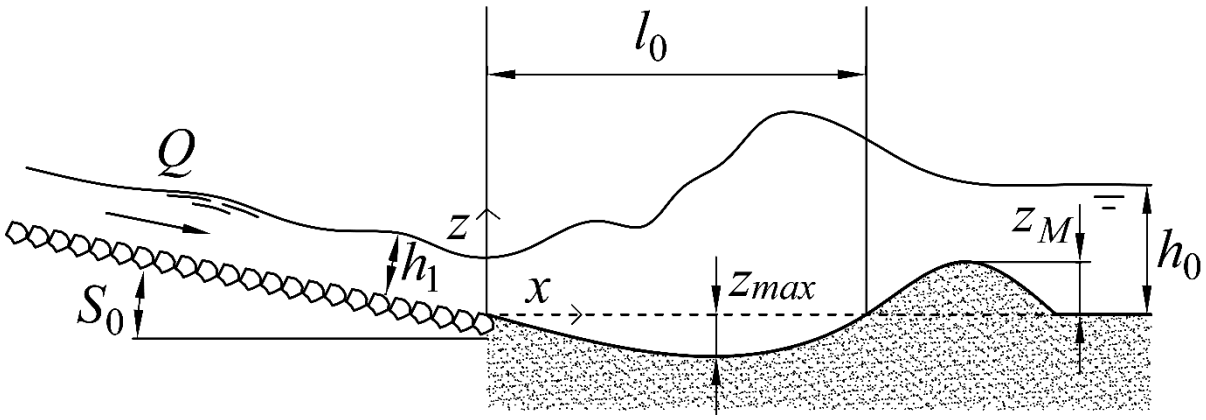

Figure 1

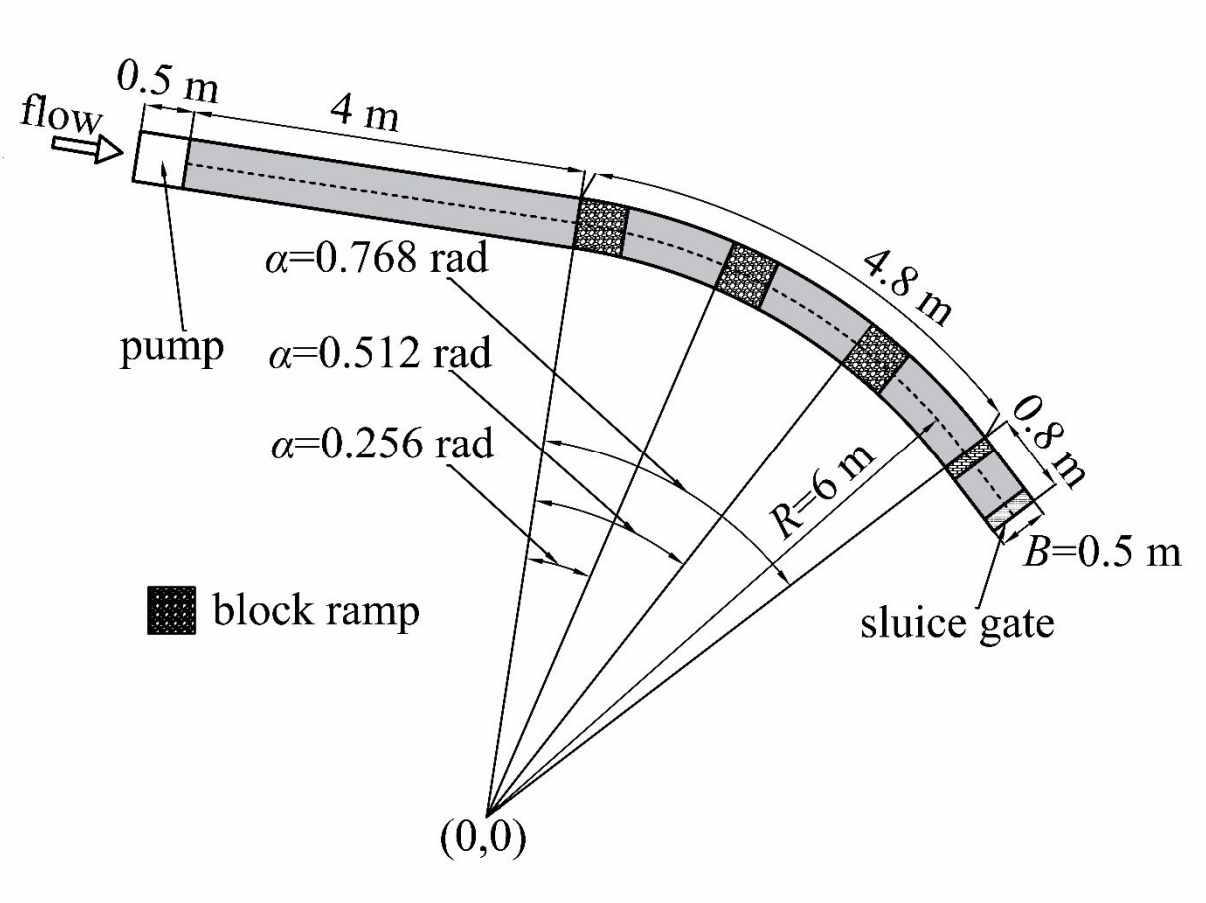
0.5 m
4 m
flow
α=0.768 rad
4.8 m
pump
α=0.512 rad
α=0.256 rad
0.8 m
R=6 m
B=0.5 m
block ramp
sluice gate
(0,0)

Figure 2

Figure 3

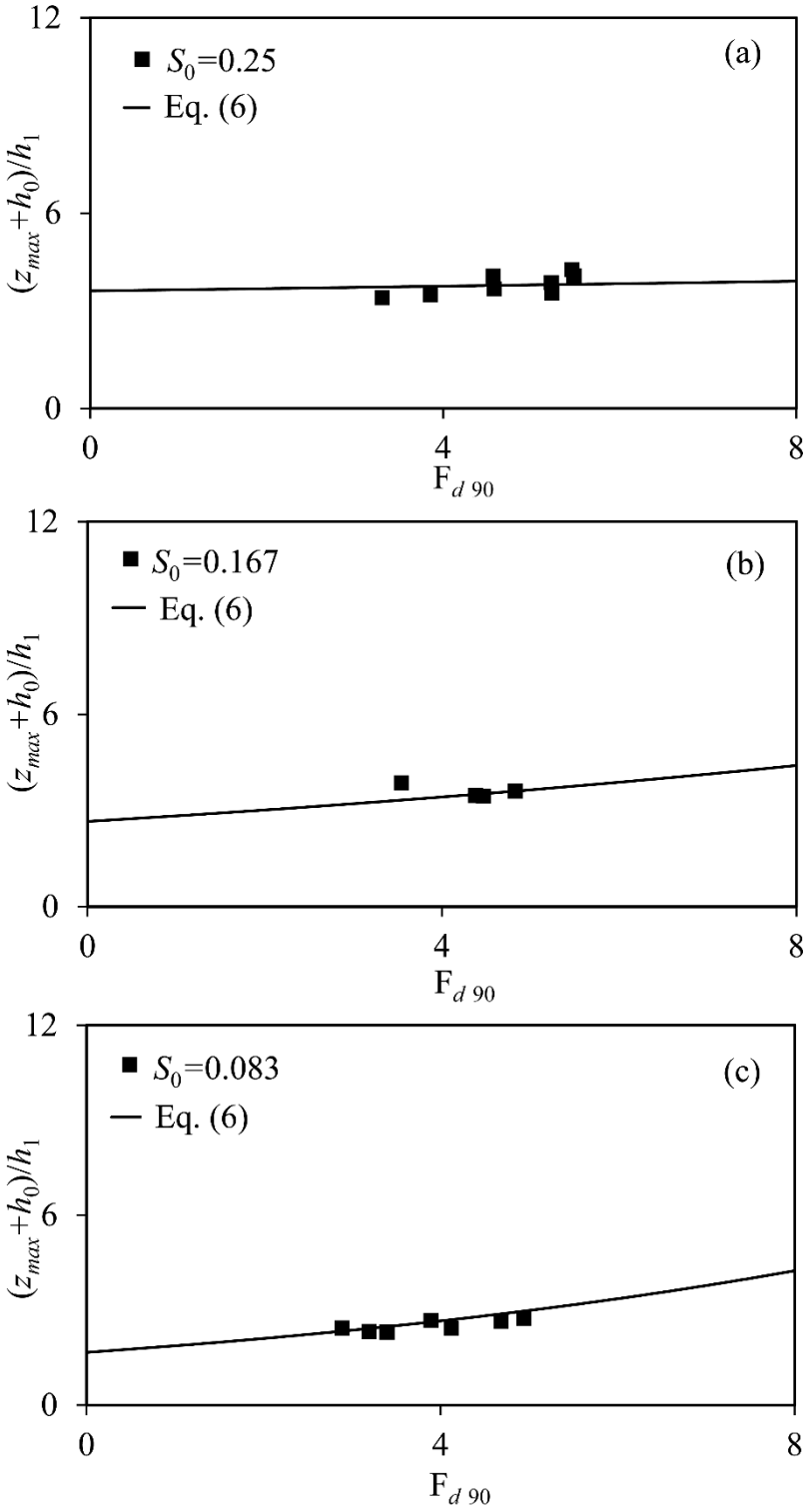
12
S_0=0.25
(a)
Eq. (6)
$(z_{max}+h_0)/h_1$
6
0
0
4
8
$F_{d\ 90}$
12
S_0=0.167
(b)
Eq. (6)
$(z_{max}+h_0)/h_1$
6
0
0
4
8
$F_{d\ 90}$
12
S_0=0.083
(c)
Eq. (6)
$(z_{max}+h_0)/h_1$
6
0
0
4
8
$F_{d\ 90}$

Figure 4

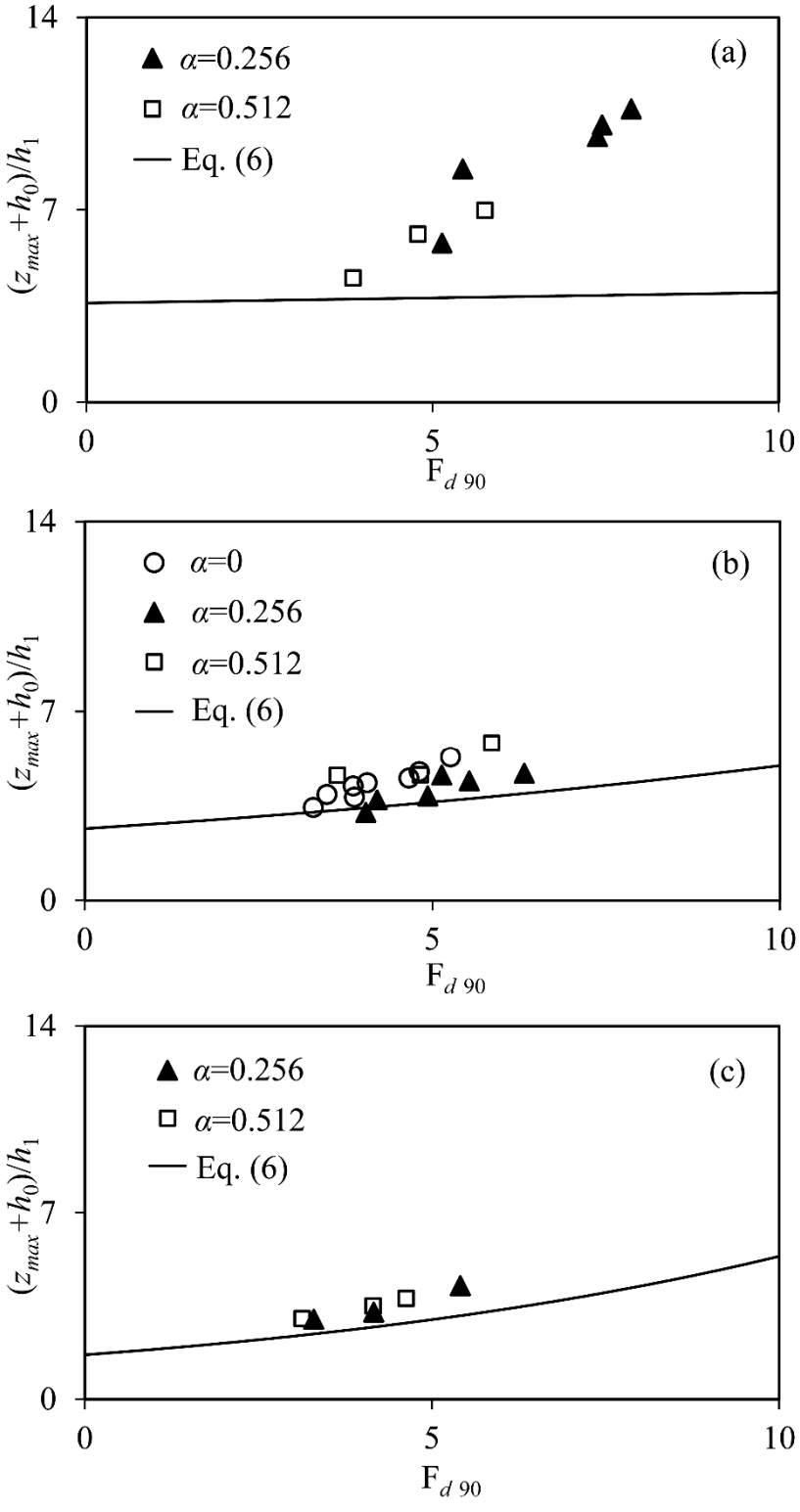
14
7
0
0
5
10
$(z_{max}+h_0)/h_1$
$F_{d\ 90}$
(a)
α=0.256
α=0.512
Eq. (6)
(b)
α=0
α=0.256
α=0.512
Eq. (6)
(c)
α=0.256
α=0.512
Eq. (6)

Figure 5

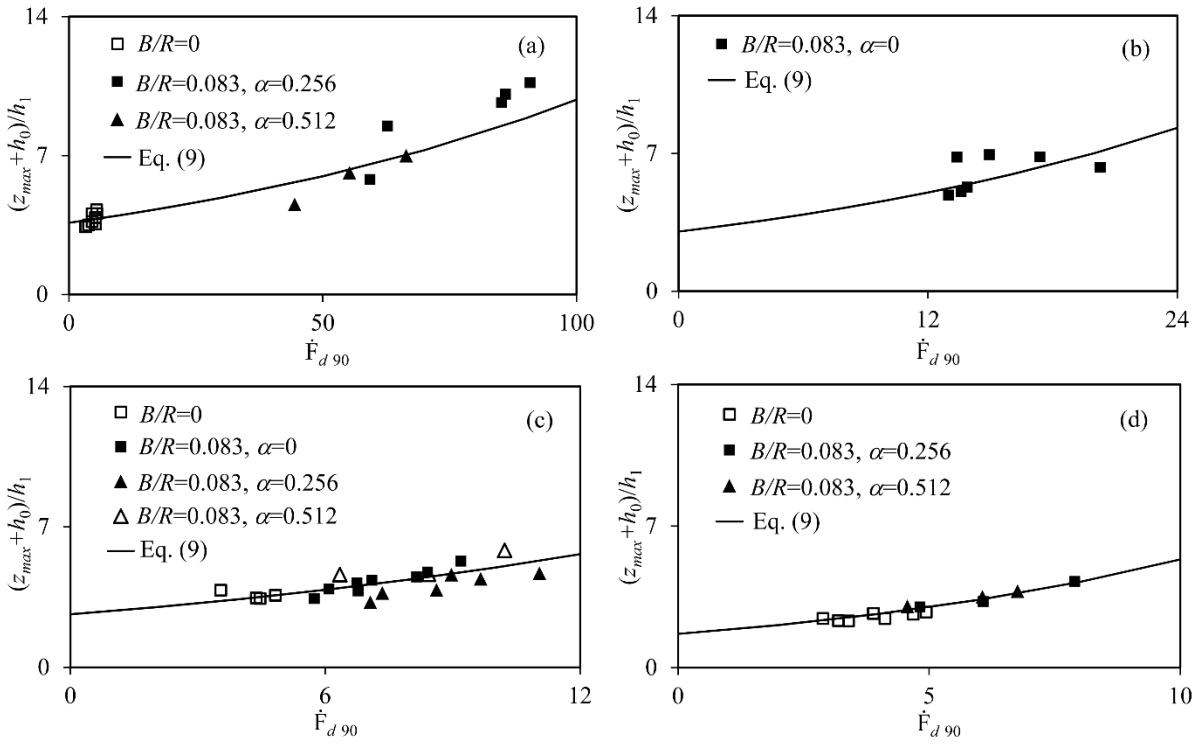
(a)
B/R=0
B/R=0.083, α=0.256
B/R=0.083, α=0.512
Eq. (9)
(b)
B/R=0.083, α=0
Eq. (9)
(c)
B/R=0
B/R=0.083, α=0
B/R=0.083, α=0.256
B/R=0.083, α=0.512
Eq. (9)
(d)
B/R=0
B/R=0.083, α=0.256
B/R=0.083, α=0.512
Eq. (9)
(z_max+h_0)/h_1
Ḟ_d 90
0
7
14
50
100
12
24
6
5
10

Figure 6

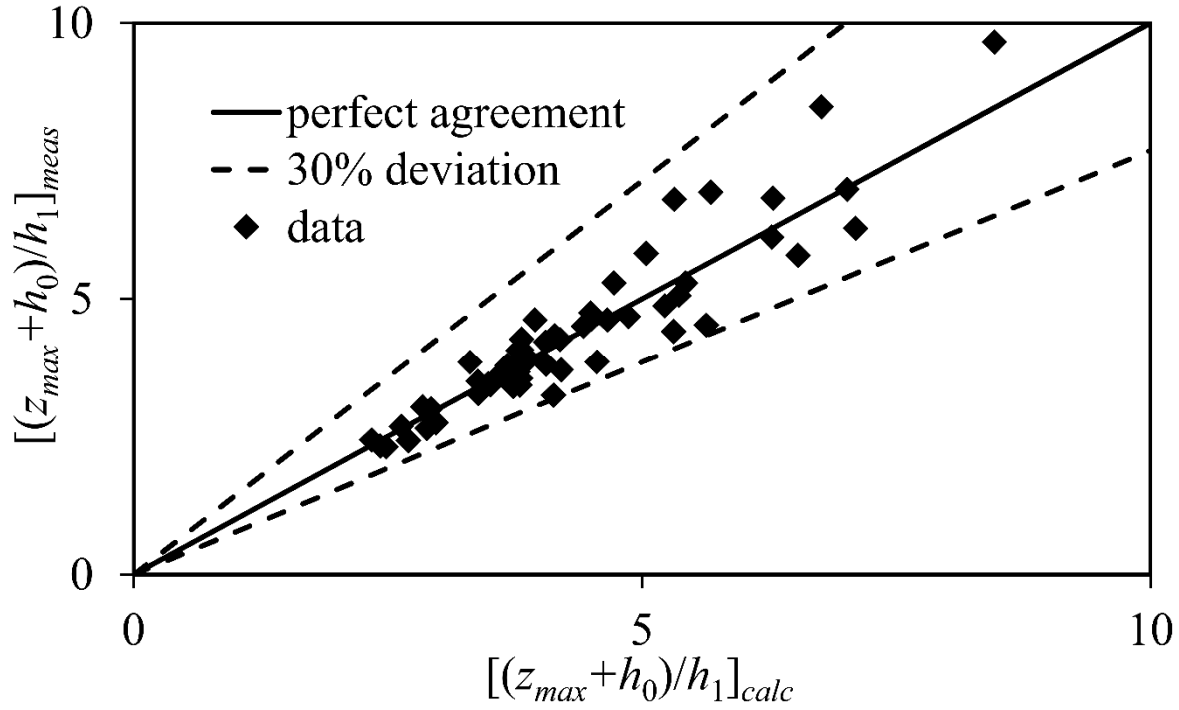
10
5
0
0
5
10
perfect agreement
30% deviation
data
$[(z_{max}+h_0)/h_1]_{meas}$
$[(z_{max}+h_0)/h_1]_{calc}$

Figure 7

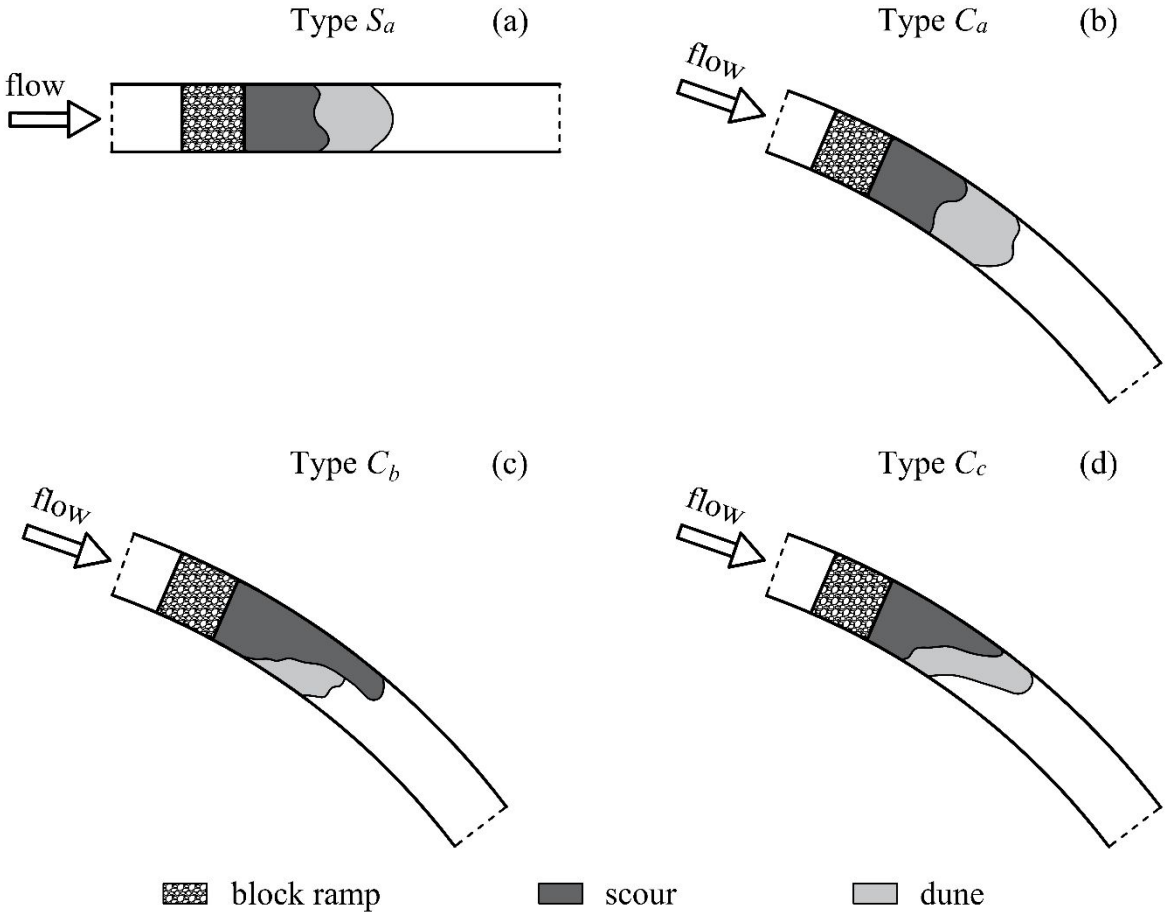
Type S_a
(a)
flow
Type C_a
(b)
flow
Type C_b
(c)
flow
Type C_c
(d)
flow
block ramp
scour
dune

Figure 8

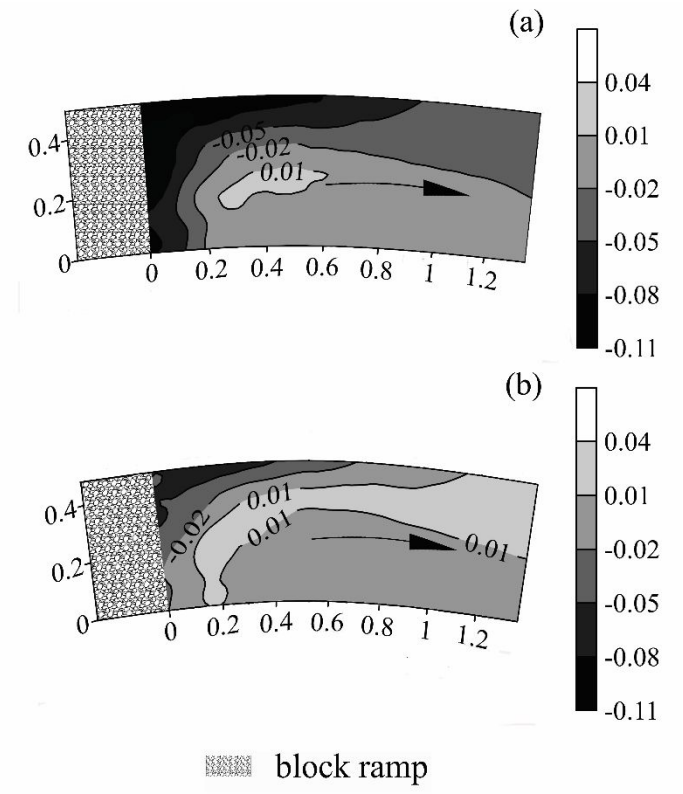
(a)
0.04
0.01
-0.02
-0.05
-0.08
-0.11
-0.05
-0.02
0.01
0.4
0.2
0
0 0.2 0.4 0.6 0.8 1 1.2
(b)
0.04
0.01
-0.02
-0.05
-0.08
-0.11
0.01
0.01
-0.02
0.01
0.4
0.2
0
0 0.2 0.4 0.6 0.8 1 1.2
block ramp

Figure 9

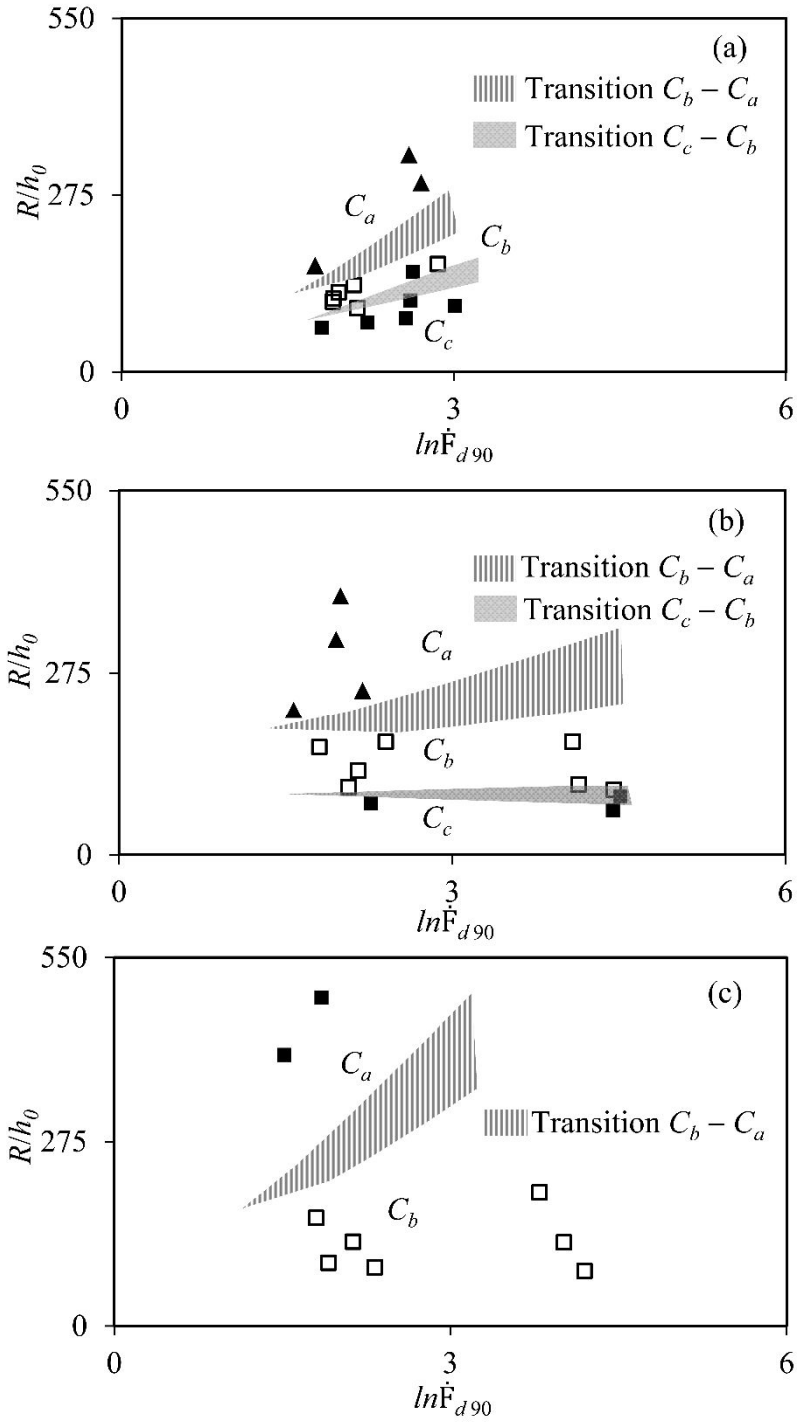
550
275
0
0
3
6
R/h_0
$ln\dot{F}_{d\,90}$
(a)
Transition $C_b - C_a$
Transition $C_c - C_b$
C_a
C_b
C_c
(b)
Transition $C_b - C_a$
Transition $C_c - C_b$
C_a
C_b
C_c
(c)
Transition $C_b - C_a$
C_a
C_b

Figure 10